The American Journal of Human Genetics, Volume *88*

Supplemental Data

Functional Screening of Alzheimer Pathology Genome-wide Association Signals in *Drosophila*

Joshua M. Shulman, Portia Chipendo, Lori B. Chibnik, Cristin Aubin, Dong Tran, Brendan T. Keenan, Patricia L. Kramer, Julie A. Schneider, David A. Bennett, Mel B. Feany, and Philip L. De Jager

Table S1. Autopsy Cohort Characteristics

As previously described in detail[12-14], participants in ROS were older Catholic nuns, priests and brothers from about 40 groups in 12 states across the United States. MAP subjects were older, community-dwelling persons from about 40 retirement communities and subsidized senior housing facilities across northeastern Illinois. Since 1993, more than 2,300 persons agreed to participate. The overall follow-up rate exceeds 90% of survivors and the overall autopsy rate exceeds 90% of decedents. Clinical diagnoses of dementia and AD were made following the recommendations of the joint working group of the National Institute of Neurologic and Communicative Disorders and Stroke and the AD and Related Disorders Association[51]. The GWAS discovery cohort included 192 ROS and 35 MAP subjects; an additional 169 ROS and 136 MAP participants comprised the replication cohort. Only self-declared subjects of non-Hispanic, European-American ancestry were studied to minimize population heterogeneity. Brain autopsies were performed across the US as previously described[12]. Persons were classified as having pathologic AD three ways: the presence of probable or highly probable AD by Consortium to Establish a Registry for Alzheimer's Disease (CERAD) based on semiquantitative estimates of highest neuritic plaque density[52], Braak stage IV–VI based on the distribution and severity of neurofibrillary tangle pathology[53], and intermediate or high likelihood of AD by National Institute on Aging (NIA)-Reagan criteria based on CERAD estimates and Braak staging[54]. A composite measure of global AD pathology was created from the resulting 15 measures (3 pathologic features in each of 5 brain regions)[15,16]. Raw counts were converted to a standard distribution by dividing each person's count by the standard deviation for that particular count and forming a summary measure by averaging the scaled scores. Because the data were skewed, square root of the averaged scaled score was used for association analyses, as in prior work[10,11].

	Discovery	Replication
n	227	305
Mean age at death (SD)	86.4 (6.7)	87.3 (6.6)
Men (%)	90 (39.6)	129 (42.3)
Mean years of education (SD)	17.8 (3.6)	16.2 (3.5)
Mean MMSE (SD)	23 (8.1)	20.8 (9.23)
NINCDS possible or probable AD (%)	87 (38.3)	130 (42.6)
Mild cognitive impairment (%)	49 (21.6)	82 (26.9)
No cognitive impairment (%)	91 (40.1)	79 (25.9)
APOE E4 allele present (%)	60 (26.4)	96 (31.5)
NIA-Reagan intermediate or high (%)	140 (61.7)	174 (57)
CERAD probable or definite (%)	147 (64.8)	194 (63.6)
Braak stage IV-VI (%)	117 (51.5)	144 (47.2)
global AD pathology (SD)[1]	0.63 (0.54)	0.70 (0.65)
neuritic plaques (SD)[1]	0.68 (0.66)	0.75 (0.81)
diffuse plaques (SD)[1]	0.83 (0.87)	0.85 (0.95)
neurofibrillary tangles (SD)[1]	0.40 (0.53)	0.53 (0.80)

[1]Mean and standard deviation of quantitative pathology measures are provided. As in prior work[16], good correlation was observed among the standardized score components and the global pathology score. For the discovery cohort, the correlations ranged from 0.32 to 0.72 (median 0.57) and the Cronbach coefficient alpha was 0.88. Similar results were obtained for the replication cohort ($0.43 < r < 0.72$, median=0.59, $\alpha=0.90$) and the pooled extension cohort ($0.40 < r < 0.72$, median=0.57, $\alpha=0.89$).

Figure S1. GWAS Quantile-Quantile and Manhattan Plots

DNA was extracted from lymphocytes or frozen post-mortem brain tissue. Genome-wide genotyping on the Illumina HumanCNV370v1C array was performed by deCODE Genetics (Reykjavik, Iceland) as part of another study, which included 178 out of the 227 subjects in an association analysis for a distinct outcome phenotype[55]. PLINK software[56] was used to implement standard quality control procedures for subjects (genotype success rate >95%, concordance of genotype-derived and reported gender, excess heterozygozity) and for SNPs (HWE $p > 1x10^{-6}$; MAF > 0.01; genotype call rate > 0.95; misshap test > $1x10^{-9}$). Subsequently, agglomerative clustering implemented within PLINK was used to detect stratification and eliminate population outliers. Following quality control, 227 subjects and 334,575 SNPs were available for analysis. The R statistical computing platform (www.r-project.org) was used to develop linear regression models relating the global AD pathology measure to age at death, and residuals were extracted to be used as the quantitative trait for SNP association analysis. The GWAS was conducted within PLINK[56] using linear regression to relate SNP genotypes to the residual quantitative trait variation in global pathology, using an additive model and including a covariate for *APOE* genotype. *APOE* genotyping was performed by Agencourt Bioscience Corporation (Beverly, MA) utilizing high throughput sequencing of codon 112 (position 3937) and codon 158 (position 4075) of exon 4 of the *APOE* gene on chromosome 19. The genomic inflation factor (λ) for the genome-wide discovery analysis was 1.009.

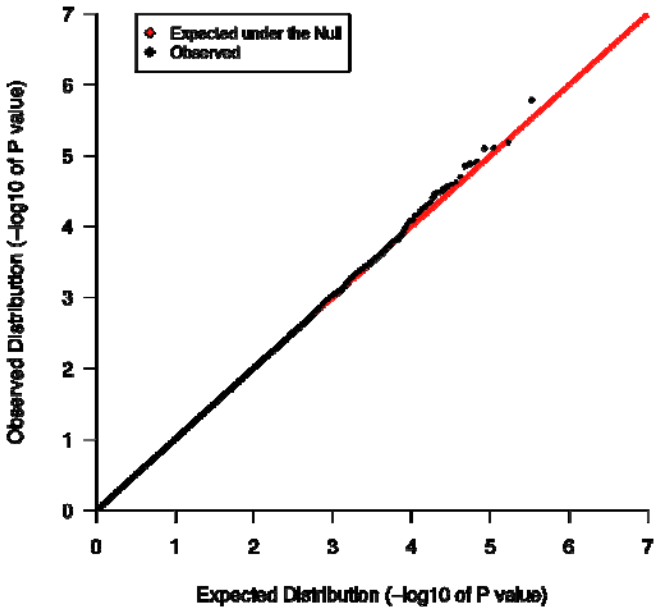

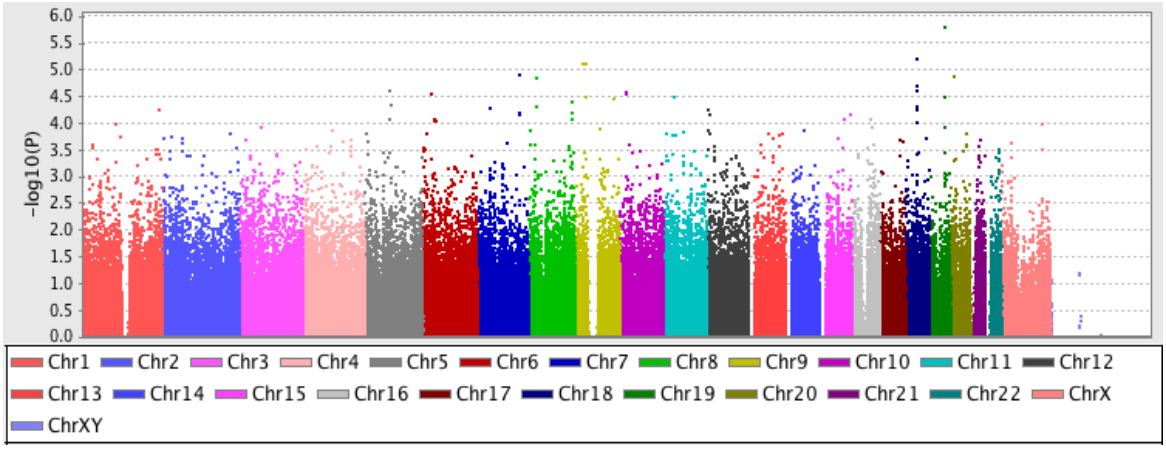

Table S2. Top GWAS Results

Full results ($p < 10^{-3}$) of the AD neuropathology GWAS are shown. In order to identify candidate genes, linkage disequilibrium based clumping, implemented within PLINK, was used to define associated regions. For each index SNP (p<0.001; MAF>0.1), additional associated SNPs (p<0.01) in linkage disequilibrium (r^2>0.5) and within 250kb proximity were used to define genomic coordinates for an associated region. The selected criteria are based on the default parameters for the SNP clumping algorithm in PLINK[56]. Any gene overlapping this range (build hg18) or within a 50kb border region was designated a candidate causal gene and considered further for functional analyses. The 50kb border region served as a conservative estimate to capture the possibility of a causal variant acting at some distance to the causal susceptibility gene.

SNP	CHR	Position	Alleles	MAF	Beta (95% CI)	P	Gene(s)
rs393569	19	45786678	C/T	0.49	0.15 (0.09 to 0.21)	$1.64x10^{-6}$	*SPTBN4 SHKBP1 LTBP4*
rs1941526	18	37906937	A/G	0.28	0.15 (0.09 to 0.22)	$6.46x10^{-6}$	*PIK3C3*
rs10970061	9	31020836	A/G	0.14	0.20 (0.12 to 0.29)	$7.83x10^{-6}$	
rs17468071	9	23669836	C/T	0.11	0.22 (0.12 to 0.31)	$7.87x10^{-6}$	*ELAVL2*
rs6131233	20	11458559	A/G	0.42	-0.13 (-0.19 to -0.08)	$1.29x10^{-5}$	
rs2280861	8	23460730	C/T	0.25	-0.16 (-0.23 to -0.09)	$1.40x10^{-5}$	*ENTPD4 SLC25A37*
rs10065260	5	77699192	C/A	0.49	0.13 (0.07 to 0.19)	$2.38x10^{-5}$	*SCAMP1 LHFPL2*
rs1935502	10	18372118	A/G	0.30	0.15 (0.08 to 0.21)	$2.66x10^{-5}$	*SLC39A12*
rs4711122	6	26866458	T/C	0.27	0.15 (0.08 to 0.22)	$2.90x10^{-5}$	
rs3824982	11	30556321	T/C	0.22	0.15 (0.08 to 0.22)	$3.22x10^{-5}$	*MPPED2*
rs12378647	9	121041535	G/A	0.35	0.14 (0.08 to 0.21)	$3.44x10^{-5}$	*DBC1*
rs7845945	8	138060351	C/T	0.46	-0.13 (-0.18 to -0.07)	$3.91x10^{-5}$	
rs16898	5	83021905	T/C	0.31	-0.13 (-0.19 to -0.07)	$4.64x10^{-5}$	*HAPLN1*
rs2108720	7	39447426	T/C	0.22	-0.16 (-0.23 to -0.08)	$5.23x10^{-5}$	*POU6F2*
rs527346	12	3255015	G/A	0.45	-0.12 (-0.18 to -0.06)	$5.72x10^{-5}$	*TSPAN9*
rs10845990	12	7861988	T/G	0.39	0.13 (0.06 to 0.19)	$6.93x10^{-5}$	*NANOG SLC2A14*
rs749229	15	96703095	T/C	0.30	0.13 (0.07 to 0.20)	$7.01x10^{-5}$	
rs1434457	15	77273979	T/C	0.23	-0.14 (-0.21 to -0.07)	$8.23x10^{-5}$	
rs9296100	6	33930843	C/T	0.22	0.14 (0.07 to 0.20)	$8.31x10^{-5}$	
rs1117361	16	55918847	T/G	0.24	0.14 (0.07 to 0.21)	$8.36x10^{-5}$	
rs324324	18	36612753	T/C	0.18	0.15 (0.08 to 0.23)	$9.57x10^{-5}$	
rs9513122	13	95798535	G/A	0.43	-0.12 (-0.18 to -0.06)	$1.70x10^{-4}$	*HS6ST3*
rs7591708	2	62875554	T/C	0.35	0.12 (0.06 to 0.18)	$1.93x10^{-4}$	*EHBP1*
rs7128063	11	83774452	A/G	0.25	-0.13 (-0.20 to -0.06)	$5.93x10^{-4}$	*DLG2*

SNP, single nucleotide polymorphism; CHR, chromosome; Position, hg build 18; Alleles, minor/major; MAF, minor allele frequency; Beta, per copy of minor allele under the additive genetic model and adjusted for age at death and *APOE ε4* genotype; P, *p*-values are unadjusted for multiple hypothesis testing.

Figure S2. Additional Enhancers of Tau Toxicity

RNAi transgenic lines were evaluated with co-expression of *Dicer2* (*Dcr2*) in order to augment activity. Compared to control animals (**A**, *GMR-Gal4,UAS-Dcr2/+*), expression of human Tau (**B**, *UAS-Tau^{V337M}/+; GMR-Gal4,UAS-Dcr2/+*) generates a reduced eye size and moderate roughened appearance. RNAi directed against *ß-Spectrin* (**C**, *UAS-Tau^{V337M}/UAS-ß-Spec.RNAi; GMR-Gal4,UAS-Dcr2/+*) [ref. 57], *heparan sulfate 6-O-sulfotransferase* (**D**, *UAS-Tau^{V337M}/+; GMR-Gal4,UAS-Dcr2/UAS-IR.Hs6st*) [ref. 58], and *discs large 1* (**E**, *UAS-Tau^{V337M}/+; GMR-Gal4,UAS-Dcr2/+*; *UAS-dlg1.IR.v41136/+*) each enhanced Tau toxicity, exacerbating the rough eye phenotype. Western blot analysis was performed to confirm that enhancers of the Tau eye phenotype did not simply increase the Tau transgene expression levels. In order to minimize the chance that modifier interactions were caused by off-target effects of RNAi, we required consistent activity of at least 2 independent RNAi lines, based on non-overlapping dsRNA constructs. The following additional RNAi lines[29,30] showed functional interactions consistent with those described above: *UAS-ß-spec-IR.v42054*, *UAS-Hs6st.IR.v42658*, *UAS-dlg1.IR.v41134*, and *UAS-dlg1.IR.JF02287*. Effects of modifiers were scored using a semi-quantitative rating scale and found to be significantly different ($p < 0.0001$) from the control condition, using pairwise independent sample t-tests (Figure S4).

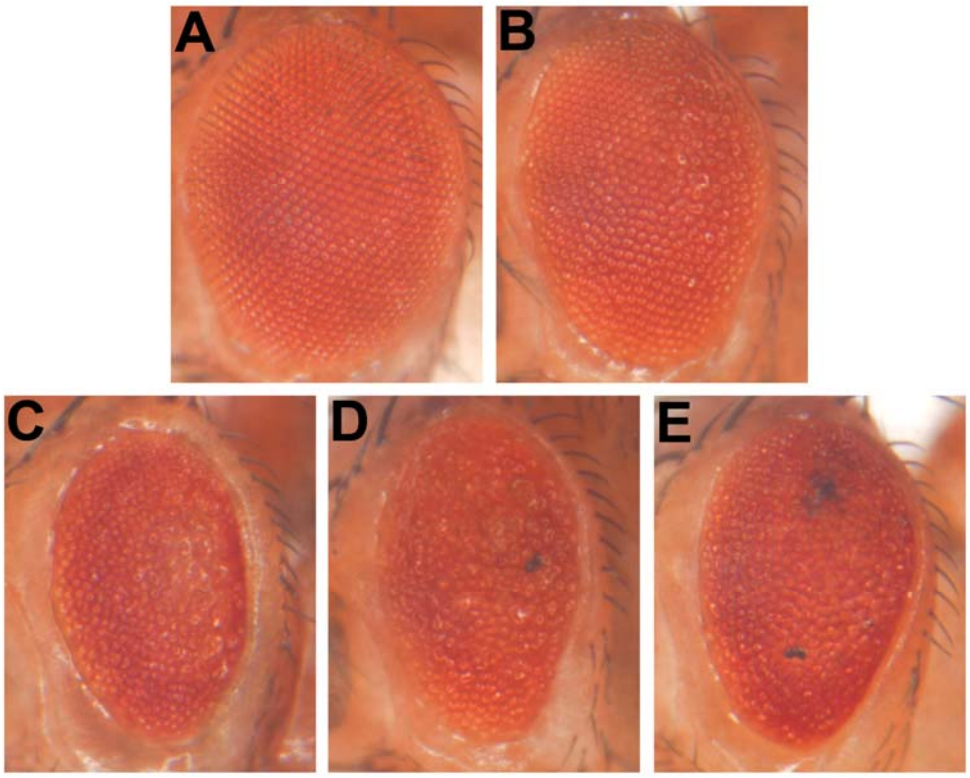

Figure S3. Tau Enhancers Are Not Significantly Toxic in Isolation

Control crosses were performed to evaluate the effect of lines discovered to enhance Tau toxicity, when expressed in the absence of the *tau*^{V337M} transgene.

(**A**) *GMR-Gal4,UAS-Dcr2/UAS-glut1.IR.v13326*
(**B**) *GMR-Gal4,UAS-Dcr2/UAS-slit.IR.v38233*
(**C**) *GMR-Gal4/+;UAS-fne.4-10B/+* [cross conducted at 23°C]
(**D**) *UAS-ß-Spec.IR/+; GMR-Gal4,UAS-Dcr2/+*
(**E**) *GMR-Gal4,UAS-Dcr2/UAS-Hs6st.IR*
(**F**) *GMR-Gal4,UAS-Dcr2/+*; *UAS-dlg1.IR.v41136/+*

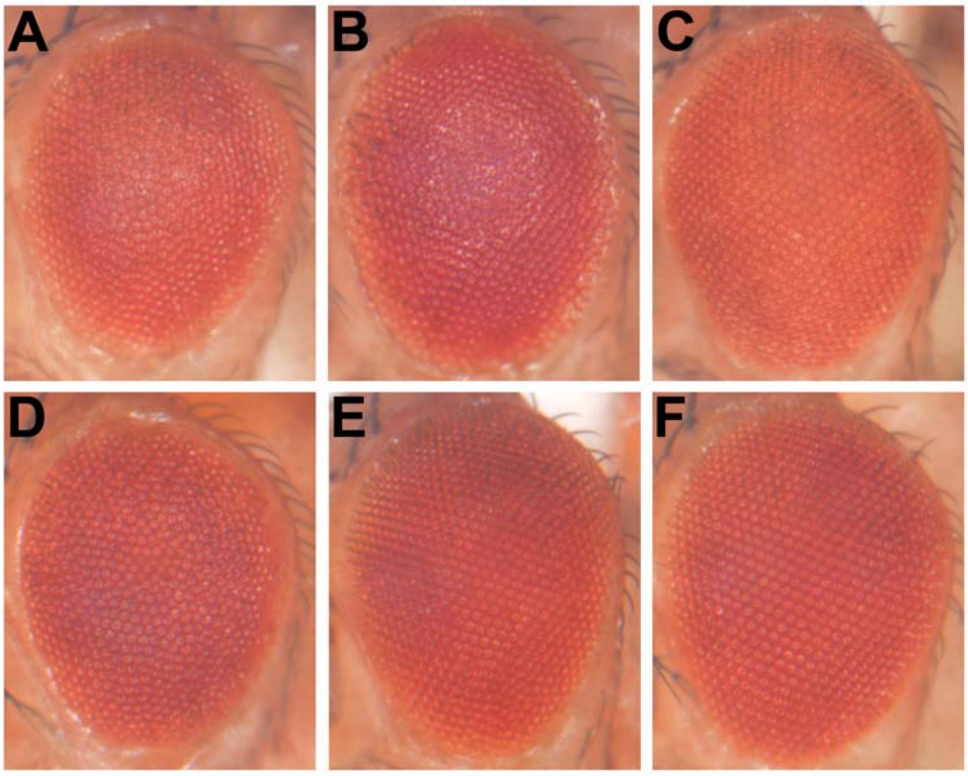

Figure S4. Quantitative Scoring of Tau Modifier Effects

Modifier effects were scored using a 6-level, semi-quantitative rating scale of rough eye severity: 0 (*wildtype* eye), 1 (*very mild rough*, <50% facet disruption), 2 (*mild rough*, 50-100% facet disruption, 0-25% reduction in eye size), 3 (*moderate rough*, 100% facet disruption, 25-50% reduction in eye size), 4 (*severe rough*, additionally with one of the following features--ommatidial fusions, darkened/discolored areas, or >50% reduction in eye size), 5 (*very severe rough*, two or more of the characteristic severe features are present). Modifiers were either tested in the presence (top, ■) or absence (bottom, ◆) of *UAS-Dcr2*, and enhancement or suppression of Tau toxicity was quantified as the average deviation in the rough eye severity score relative to control Tau transgenic flies, *UAS-Tau^{V337M}/+; GMR-Gal4,UAS-Dcr2/+* (□) or *UAS-Tau^{V337M}/+; GMR-Gal4/+* (◇), respectively. Using pair-wise independent sample t-tests, all modifiers effects were found to be highly significant ($p < 0.0001$). In order to facilitate comparisons of modifier effects relative to the two control conditions, the results were centered at 0, based on the mean control score. Mean and 95% confidence intervals are shown. Gain-of-function in either *slit* (2) or *Glut1* (3) and loss-of-function in *fne* (4) suppressed Tau toxicity; whereas enhancement of Tau toxicity was observed with gain-of-function in *fne* (5) and loss-of-function in *slit* (7), *Glut1* (8), *Hs6st* (9), *dlg1* (10), or *ß-spectrin* (11).

Genotype	# flies scored
(1) *UAS-Tau^{V337M}/+; GMR-Gal4/+*	n=43
(2) *UAS-Tau^{V337M}/+; GMR-Gal4/+;UAS-sli.B/+*	n=77
(3) *UAS-Tau^{V337M}/+; GMR-Gal4/+; Glut1^{d05758}/+*	n=51
(4) *UAS-Tau^{V337M}/+; GMR-Gal4/UAS-fne.IR.v101508*	n=56
(5) *UAS-Tau^{V337M}/+; GMR-Gal4/+;UAS-fne.4-10B/+*	n=24
(6) *UAS-Tau^{V337M}/+; GMR-Gal4,UAS-Dcr2/+*	n=37
(7) *UAS-Tau^{V337M}/+; GMR-Gal4,UAS-Dcr2/UAS-slit.IR.v38233*	n=95
(8) *UAS-Tau^{V337M}/+; GMR-Gal4,UAS-Dcr2/UAS-glut1.IR.v13326*	n=81
(9) *UAS-Tau^{V337M}/+; GMR-Gal4,UAS-Dcr2/UAS-IR.Hs6st*	n=83
(10) *UAS-Tau^{V337M}/+; GMR-Gal4,UAS-Dcr2/+; UAS-dlg1.IR.v41136/+*	n=42
(11) *UAS-Tau^{V337M}/UAS-ß-Spec.RNAi; GMR-Gal4,UAS-Dcr2/+*	n=83

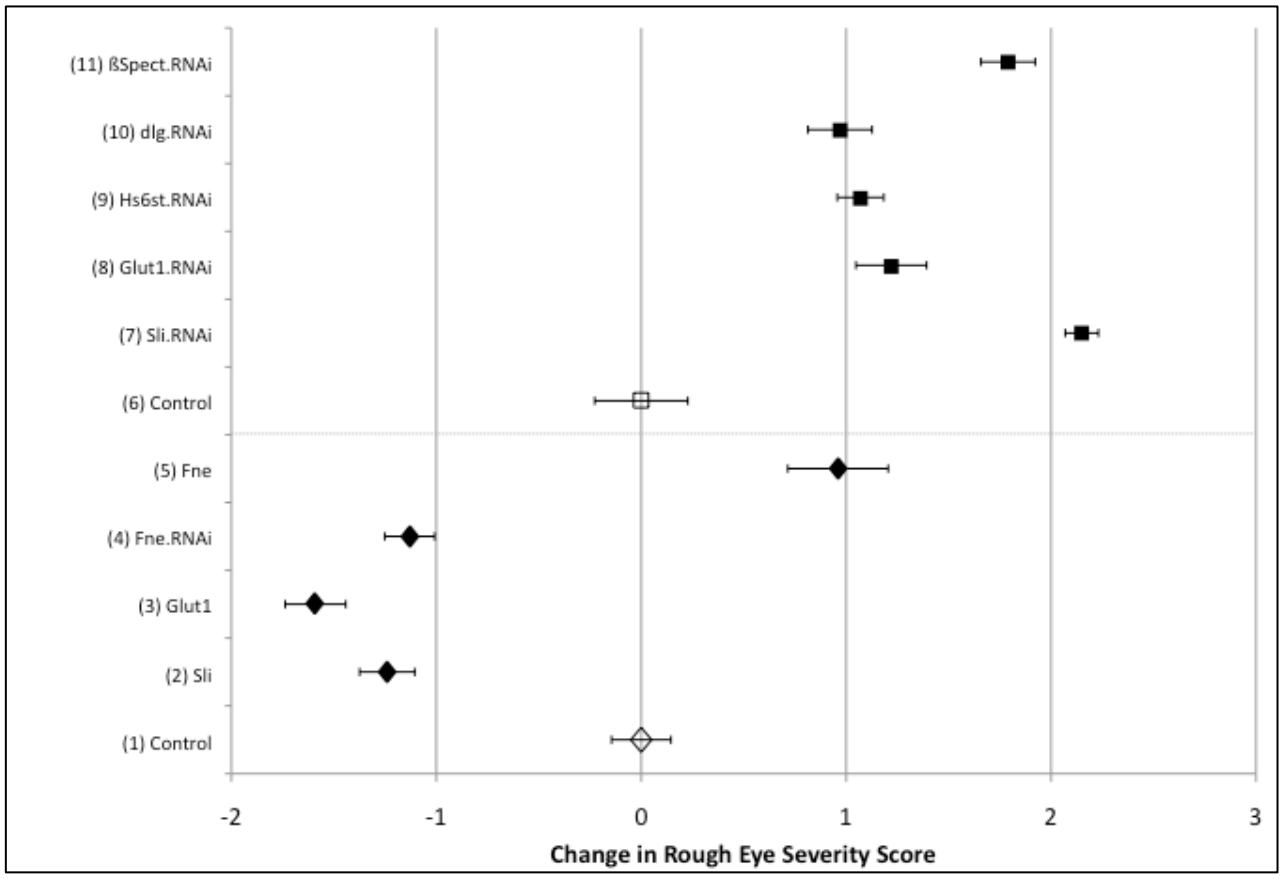

Table S3. Replication Analysis of Functionally Validated Loci

For replication, SNPs were genotyped using matrix-assisted laser desorption-ionization time-of-flight mass spectrometry on a MassARRAY platform (Sequenom). Association analysis in the replication and joint cohorts was otherwise performed as described for the discovery stage analysis (see Figure S1), using PLINK software[56].

			Replication (n~305)		Joint (n~532)	
GENE	**SNP**	**A1**	**BETA (95% CI)**	**P**	**BETA (95% CI)**	**P**
SLIT3	rs297808	G	-0.055 (-0.117 to 0.008)	0.087	0.007 (-0.037 to 0.052)	0.741
ELAVL2	rs17468071	C	0.020 (-0.075 to 0.115)	0.681	0.095 (0.027 to 0.162)	6.42E-03
DLG2	rs7128063	A	-0.038 (-0.103 to 0.027)	0.257	-0.067 (-0.114 to -0.020)	5.56E-03
SLC2A14	rs10845990	T	0.069 (0.008 to 0.131)	**0.027**	0.098 (0.055 to 0.140)	8.09E-06
HS6ST3	rs9513122	G	0.025 (-0.036 to 0.085)	0.428	-0.028 (-0.072 to 0.016)	0.214
SPTBN4	rs393569	T	-0.005 (-0.065 to 0.054)	0.861	-0.058 (-0.099 to -0.016)	6.46E-03

A1, minor/reference allele

SUPPLEMENTAL REFERENCES

51. McKhann, G., Drachman, D., Folstein, M., Katzman, R., Price, D., and Stadlan, E.M. (1984). Clinical diagnosis of Alzheimer's disease: report of the NINCDS-ADRDA Work Group under the auspices of Department of Health and Human Services Task Force on Alzheimer's Disease. Neurology 34, 939-944.

52. Mirra, S.S., Heyman, A., McKeel, D., Sumi, S.M., Crain, B.J., Brownlee, L.M., Vogel, F.S., Hughes, J.P., van Belle, G., and Berg, L. (1991). The Consortium to Establish a Registry for Alzheimer's Disease (CERAD). Part II. Standardization of the neuropathologic assessment of Alzheimer's disease. Neurology 41, 479-486.

53. Braak, H., and Braak, E. (1991). Neuropathological stageing of Alzheimer-related changes. Acta Neuropathol 82, 239-259.

54. The National Institute on Aging, and Reagan Institute Working Group on Diagnostic Criteria for the Neuropathological Assessment of Alzheimer's Disease. (1997). Consensus recommendations for the postmortem diagnosis of Alzheimer's disease. The National Institute on Aging, and Reagan Institute Working Group on Diagnostic Criteria for the Neuropathological Assessment of Alzheimer's Disease. Neurobiol Aging 18, S1-2.

55. Kramer, P.L., Xu, H., Woltjer, R.L., Westaway, S.K., Clark, D., Erten-Lyons, D., Kaye, J.A., Welsh-Bohmer, K.A., Troncoso, J.C., Markesbery, W.R., et al. (2010). Alzheimer disease pathology in cognitively healthy elderly: A genome-wide study. Neurobiol Aging Epub, 10.1016/j.neurobiolaging.2010.1001.1010.

56. Purcell, S., Neale, B., Todd-Brown, K., Thomas, L., Ferreira, M., Bender, D., Maller, J., Sklar, P., de Bakker, P., Daly, M., et al. (2007). PLINK: a tool set for whole-genome association and population-based linkage analyses. Am J Hum Genet 81, 559-575.

57. Hulsmeier, J., Pielage, J., Rickert, C., Technau, G.M., Klambt, C., and Stork, T. (2007). Distinct functions of alpha-Spectrin and beta-Spectrin during axonal pathfinding. Development 134, 713-722.

58. Kamimura, K., Koyama, T., Habuchi, H., Ueda, R., Masu, M., Kimata, K., and Nakato, H. (2006). Specific and flexible roles of heparan sulfate modifications in Drosophila FGF signaling. J Cell Biol 174, 773-778.